Analytical framework for incorporating uncertainties into design optimization of tuned mass dampers

Mario Argenziano[a,*], Riccardo Cavuoto[b], Yoshiki Ikeda[c]

[a]*Department of Engineering, University of Palermo, Palermo, Sicily, Italy*
[b]*Department of Structures for Engineering and Architecture, University of Naples Federico II, Napoli, Campania, Italy*
[c]*Disaster Prevention Research Institute, Kyoto University, Gokasho, Uji, Kyoto, Japan*

Abstract

Tuned mass dampers (TMDs) are effective and well-established solutions for mitigating the dynamic responses of structures exposed to seismic events and extreme winds. Traditionally, their design employs deterministic mechanical parameters that account for randomness exclusively in the input excitations. Furthermore, conventional TMD optimization strategies aim to minimize the structural response of the so-called primary system using a fully deterministic definition of the design parameters of the absorber. However, real-world structural characteristics are inherently subject to aleatory uncertainty because of uneven material composition, manufacturing margins of error, environmental shifts, and gradual degradation. Neglecting these natural fluctuations can cause a deterministically calibrated TMD to lose synchronization with the main structure, thereby compromising system efficiency and leading to sub-optimal configurations. To overcome these significant limitations, this paper introduces a fully stochastic analytical framework for TMD design that explicitly considers the random variability of the constitutive properties of the absorber. The core approach of this proposed framework is the unprecedented integration of the pole allocation method applied to TMD systems into a probabilistic setting within a fully analytical framework. Treating the design as an inverse problem, the approach initially defines the target structural response, namely, the ideal modal frequencies and damping ratios, which are mathematically recognized as poles. Subsequently, it works backwards to calculate the required physical properties of the passive absorber, incorporating the variance of its mechanical parameters.

This research shifts the design paradigm of such systems from a deterministic model to a fully stochastic domain. Thus, it provides a novel engineering tool for comprehensively managing parameter uncertainties, paving the way for more resilient and robust TMD devices.

Keywords:
structural dynamics, vibration control, tuned mass damper, pole allocation method, uncertainties in mechanical parameters

Abbreviations

TMD, tuned mass damper; DoF, degree-of-freedom; MC, Monte Carlo simulations; PDF, probability density function; CDF, cumulative distribution function.

1. Introduction

Over the past few decades, architectural and structural engineering communities have attempted to address the increasingly challenging task of elevating building safety profiles while concurrently limiting carbon emissions and material consumption. This dual necessity has catalyzed the development of advanced structural frameworks and the

*Corresponding author
Email address: mario.argenziano@unipa.it (Mario Argenziano)

design of novel building materials to safeguard buildings and civil structures against severe environmental loads such as seismic and wind excitations. To this aim, researchers have introduced and investigated various passive control strategies. Among them, passive tuned mass dampers (TMDs) [1, 2, 3, 4, 5, 6], which feature high reliability, relatively easy assembly, cost-effectiveness, and independence from external excitations, are considered optimal for mitigating the dynamic response of structures in comparison to active or semi-active control systems, which always require a feedback system to work.

A TMD comprising a supplementary mass, spring element, and damping mechanism, is mounted on a main structure to regulate its dynamic behavior. The fundamental concept relies on drawing vibrational energy away from the primary structure and dissipating it through the motion of an auxiliary mass, which is often designated as a passive dynamic absorber that requires the precise optimization of the damping and tuning parameters. In the design phase, the physical properties of the primary structure (i.e., inherent damping, mass, and stiffness) are considered prescribed deterministic constants, which leaves the mechanical characteristics of the secondary system to be defined as design variables.

The concept of the TMD originated from Frahm's dynamic absorbers [7] within the mechanical engineering field. Subsequently, Den Hartog [1] formulated the optimal parameters for undamped main systems by exploiting the so-called *invariant points* or *fixed points* theory and by providing compact closed-form solutions for the TMD design parameters. Although this optimization procedure is very old, it is employed in current pre-sizing design procedures because of its relative simplicity and reliability. Several numerical or approximate methods based on Den Hartog's optimization strategy have been introduced for the case where the damping of the primary system is non-negligible [8, 9, 10, 11]. More recently, the scientific community has demonstrated a keen interest in this topic. Within this framework, a large number of single-objective (e.g. H_∞ and H_2) or multicriteria optimization strategies [12, 13, 14, 15, 16, 17, 18, 19, 20] have been conceived and discussed, thereby producing several analytical or numerical formulations for the *ad hoc* design of TMDs that can withstand various types of excitations.

Further extensive efforts have been invested not only in defining optimal formulations for TMD structures but also in conceptualizing more complex configurations by integrating TMDs with other vibration control techniques, such as inerters [21, 22] or base-isolation systems [23].

Although this topic has been investigated extensively, most existing optimization methods heavily rely on the assumption that the constitutive parameters of two degrees-of-freedom (DoF) systems are deterministic. Consequently, while these formulations provide useful and widely used design guidelines even for the case of stochastic excitation inputs [24, 10, 3, 6], they do not consider the natural fluctuations of parameters in actual physical structures. In practice, structural characteristics are subject to randomness [25, 26, 27, 28] caused by uneven material compositions, manufacturing margins of error, simplified theoretical models, environmental changes (e.g., variations in humidity and temperature), and gradual structural degradation over time. Such unpredictable aspects can alter the damping and stiffness of the system, causing the actual values to vary when compared to those defined using the optimization procedure. Thus, a TMD calibrated using strictly deterministic models can lose its synchronization with the main structure. This de-tuning effect can compromise the efficiency of the TMD and worsen the dynamic response of the overall system, thereby resulting in *de facto* sub-optimal configurations.

Therefore, incorporating the randomness of the design variables (e.g., the stiffness and damping of the absorber) directly into optimization strategies is a crucial yet delicate issue that requires attention. In recent years, several researchers [29, 30, 31] have demonstrated the importance of considering uncertainties in mechanical parameters when designing TMD systems. Their research highlights the limits of standard optimization methods and suggests the need to develop a robust strategy that can clearly address this problem. However, to the best of the authors' knowledge, a complete optimization method that can consider the uncertain properties of the absorber mass remains lacking. To bridge this gap and motivated by the critical need to prevent severe structural de-tuning —wherein manufacturing errors and environmental shifts degrade conventional TMD performance— this paper proposes a rigorous analytical approach that directly includes the random nature of the constitutive properties of the absorber, adopting normal Gaussian functions to estimate their probability distributions. To the best of the authors' knowledge, this is the first study to present this approach. To define the target structural response *a priori*, the provided framework leverages the implementation of the so-called pole allocation method [32]. This method is traditionally considered a tool for active control and has been successfully re-shaped and adapted to design passive vibration control for discrete structural systems [33, 34, 35]. Unlike the standard approach where the properties of the damper are estimated first and the structural response is calculated later, this design approach is treated as an inverse problem. The process first defines

the desired behavior of the structure, focusing specifically on its ideal (somehow optimal) modal frequencies and damping ratios. These performance targets are mathematically recognized in the field of structural dynamics as the poles of the mechanical system. Once these targets are set, the approach works backwards to calculate the exact physical properties (i.e., stiffness and damping) required by the passive absorber to meet these goals. Building on these concepts, a major contribution of this study is the unprecedented integration of the pole allocation technique into a fully probabilistic domain, thereby explicitly accounting for the random variability in the design parameters of the absorber. To this end, a closed-form probability density function (PDF) of the poles of the mechanical system is derived by incorporating the probability distribution of the stiffness and damping of the absorber. The results are represented numerically and discussed by comparing them with output parameters derived by the simple and well-established Den Hartog approach for the design of TMD systems. Unlike the previous applications of the pole allocation method for discrete systems, the target dynamic response cannot be evaluated as a single deterministic value. Instead, it is characterized by a PDF that depends on the average and variance values of the design parameters, namely, the stiffness and damping of the secondary mass.

Thus, by shifting the design paradigm from a conventional deterministic approach to a fully stochastic inverse problem, we believe that this work may pave the way for more resilient structural control methodologies. Ultimately, this is expected to offer researchers, engineers, and designers a powerful analytical framework for managing parameter uncertainties with mathematical rigour, thereby facilitating enhanced and robust engineering designs of TMD structures.

The remainder of this paper is organized as follows: Section 2 presents the governing equations and the application of the pole allocation method to the 2-DoF system in a deterministic framework. Section 3 evaluates the effects of uncertainties in the mechanical parameters on the overall structural response of TMD systems. Section 4 provides a fully analytical theoretical framework for the pole allocation method in a stochastic environment by explicitly incorporating the randomness of the TMD design parameters. Finally, Section 5 summarizes the concluding remarks and outlines the future perspectives for the present study.

2. Modeling strategy

2.1. Statement of the problem: dynamics equations

The dynamics of a TMD can be investigated effectively in a preliminary design stage through a lumped-mass 2-DoF mechanical linear system shown in Figure 1.

Let $u_1(t)$ and $u_2(t)$ represent the displacements of masses m_1 and m_2 relative to the ground, respectively. Assuming $\ddot{u}_g(t)$ is the input ground acceleration exciting the system, and k_1, k_2 and c_1, c_2 represent the stiffness and damping coefficients of the two DoF, the equations of motion for this 2-DoF system can be expressed as

$$\begin{cases} m_1\ddot{u}_1(t) + (c_1 + c_2)\dot{u}_1(t) - c_2\dot{u}_2(t) + \\ \quad + (k_1 + k_2)u_1(t) - k_2u_2(t) = -m_1\ddot{u}_g(t) \\ m_2\ddot{u}_2(t) - c_2\dot{u}_1(t) + c_2\dot{u}_2(t) + \\ \quad - k_2u_1(t) + k_2u_2(t) = -m_2\ddot{u}_g(t) \end{cases}, \tag{1}$$

where the dot indicates the time derivative.

These equations can be conveniently expressed in the matrix form as

$$\begin{aligned} &\begin{bmatrix} m_1 & 0 \\ 0 & m_2 \end{bmatrix}\begin{bmatrix} \ddot{u}_1(t) \\ \ddot{u}_2(t) \end{bmatrix} + \begin{bmatrix} c_1 + c_2 & -c_2 \\ -c_2 & c_2 \end{bmatrix}\begin{bmatrix} \dot{u}_1(t) \\ \dot{u}_2(t) \end{bmatrix} + \\ &+ \begin{bmatrix} k_1 + k_2 & -k_2 \\ -k_2 & k_2 \end{bmatrix}\begin{bmatrix} u_1(t) \\ u_2(t) \end{bmatrix} = -\begin{bmatrix} m_1 \\ m_2 \end{bmatrix}\ddot{u}_g(t) \quad , \end{aligned} \tag{2}$$

A set of dimensionless parameters are adopted by invoking the so-called Buckingham π-theorem to generalise the dynamic behavior of the system and reduce the number of independent variables. To this end, we introduce the following dimensionless ratios: the mass ratio $\mu = m_2\, {m_1}^{-1}$, stiffness ratio $f = k_2\, {k_1}^{-1}$, and primary and secondary damping ratios $\xi_1 = c_1(2\, m_1\, \omega_1)^{-1}$ and $\xi_2 = c_2(2\, m_2\, \omega_2)^{-1}$, respectively. Recalling that the uncoupled natural squared

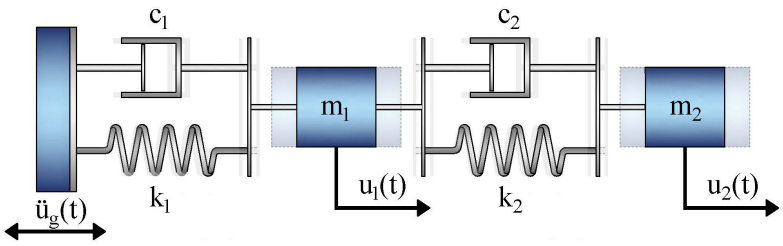


Figure 1: Schematic of a 2-DoF damped spring–mass system subjected to base excitation (ground acceleration $\ddot{u}_g(t)$).

circular frequencies of the two DoFs are respectively defined as ${\omega_1}^2 = k_1 {m_1}^{-1}$ and ${\omega_2}^2 = k_2 {m_2}^{-1}$, the mechanical parameters of the system can be expressed in terms of the primary mass and frequency (m_1 and ω_1, respectively) and the previously-defined dimensionless ratios. Therefore, Equation (1) can be rewritten as

$$\begin{aligned} &\ddot{u}_1(t) + 2\omega_1 \left(\xi_1 + \xi_2 \sqrt{f\mu}\right) \dot{u}_1(t) - 2\omega_1 \xi_2 \sqrt{f\mu}\, \dot{u}_2(t) + \\ &\quad + \omega_1^2 (1+f) u_1(t) - \omega_1^2 f u_2(t) = -\ddot{u}_g(t) \\ &\mu \ddot{u}_2(t) - 2\omega_1 \xi_2 \sqrt{f\mu}\, \dot{u}_1(t) + 2\omega_1 \xi_2 \sqrt{f\mu}\, \dot{u}_2(t) + \\ &\quad - \omega_1^2 f u_1(t) + \omega_1^2 f u_2(t) = -\mu \ddot{u}_g(t) \end{aligned} \quad . \tag{3}$$

To convert this system into a state-space representation, we define a set of four state variables collected in the state vector $\mathbf{z}(t) = \begin{bmatrix} u_1 & u_2 & \dot{u}_1 & \dot{u}_2 \end{bmatrix}^T$.

The system can be expressed in the standard state-space form by isolating the highest-order derivatives ($\ddot{u}_1$ and $\ddot{u}_2$) from the equations of motion and dividing the second equation by the mass ratio μ.

$$\dot{\mathbf{z}}(t) = \mathbf{A}\, \mathbf{z}(t) + \mathbf{B}\, \ddot{u}_g(t) \quad , \tag{4}$$

where $\mathbf{A}$ represents the system matrix (4×4) and $\mathbf{B}$ represents the input matrix (4×1), which are expressed as

$$\begin{aligned} \mathbf{A} &= \begin{bmatrix} 0 & 0 & 1 & 0 \\ 0 & 0 & 0 & 1 \\ -\omega_1^2(1+f) & \omega_1^2 f & -2\omega_1 \left(\xi_1 + \xi_2 \sqrt{f\mu}\right) & 2\omega_1 \xi_2 \sqrt{f\mu} \\ \omega_1^2 f \mu^{-1} & -\omega_1^2 f \mu^{-1} & 2\omega_1 \xi_2 \sqrt{f\mu^{-1}} & -2\omega_1 \xi_2 \sqrt{f\mu^{-1}} \end{bmatrix}, \\ \mathbf{B} &= \begin{bmatrix} 0 \\ 0 \\ -1 \\ -1 \end{bmatrix} \quad . \end{aligned} \tag{5}$$

To obtain the characteristic equation of the system, we set the determinant of the system matrix $\mathbf{A} - \mathbf{I}\,\lambda$ to zero.

$$\det(\mathbf{A} - \mathbf{I}\,\lambda) = 0 \quad , \tag{6}$$

where $\mathbf{I}$ is a 4×4 identity matrix. Expanding Equation (6) yields the secular equation in terms of the system eigenvalues (i.e., the poles) λ as

$$\begin{aligned}
&\lambda^4 + 2\left[\xi_1 + \left(\sqrt{f\mu^{-1}} + \sqrt{f\mu}\right)\xi_2\right]\omega_1\lambda^3 + \\
&+ \frac{\left(f + \mu + f\mu + 4\sqrt{f\mu}\,\xi_1\xi_2\right)\omega_1^2}{\mu}\lambda^2 + \\
&+ \frac{2\left(f\xi_1 + \sqrt{f\mu}\,\xi_2\right)\omega_1^3}{\mu}\lambda + \frac{f\omega_1^4}{\mu} = 0 \quad .
\end{aligned} \tag{7}$$

2.2. Pole allocation method

The pole allocation method is a powerful technique used to *a priori* prescribe a specific dynamic behavior to the 2-DoF system. The core principle of this method is to force the roots of the characteristic equation of the actual system to match a set of desired target poles. For a 2-DoF system, the target characteristic polynomial can be defined by assuming that the system behaves as two decoupled single-degree-of-freedom (SDoF) oscillators. Let Ω_1 and Ω_2 represent the natural modal frequencies, and let h_1 and h_2 represent the corresponding damping ratios of these two target modes. Consequently, the desired characteristic equation can be expressed as a product of these two independent second-order polynomials.

$$\left(\lambda^2 + 2h_1\Omega_1\lambda + \Omega_1^2\right)\left(\lambda^2 + 2h_2\Omega_2\lambda + \Omega_2^2\right) = 0 \quad . \tag{8}$$

In dynamic analysis involving complex eigenvalues, the modal damping ratios h_i are evaluated directly from the roots of the Equation (8) using the relationship

$$h_i = -\frac{\mathrm{Re}[\lambda_i]}{|\lambda_i|} \quad , \tag{9}$$

where $\mathrm{Re}[\lambda_i]$ and $|\lambda_i|$ represent the real part and absolute norm of the complex eigenvalue, respectively, with the latter corresponding to the undamped modal frequency Ω_i of the i-th mode.

Therefore, expanding Equation (8) and grouping terms by the powers of the unknown poles λ, the target polynomial takes the explicit form

$$\begin{aligned}
&\lambda^4 + 2(h_1\Omega_1 + h_2\Omega_2)\lambda^3 + \left(\Omega_1^2 + \Omega_2^2 + 4h_1h_2\Omega_1\Omega_2\right)\lambda^2 + \\
&+ 2\Omega_1\Omega_2(h_1\Omega_2 + h_2\Omega_1)\lambda + \Omega_1^2\Omega_2^2 = 0
\end{aligned} \quad . \tag{10}$$

Equating the coefficients of Equation (8) with those of the general analytical characteristic Equation (6) yields a system of nonlinear algebraic equations in terms of the unknown mechanical dimensionless ratios. Solving this system permits the analytical determination of the mechanical parameters, such as the mass ratio μ, stiffness ratio f, natural frequency ω_1, or damping coefficients ξ_1 and ξ_2 required to precisely place the poles of the coupled system at the target locations in the complex plane.

Furthermore, the mathematical problem simplifies significantly if the inherent damping of the primary structure is assumed to be negligible ($\xi_1 \to 0$, which is physically reasonable for real-life civil engineering structures when compared to the substantial damping introduced by the absorber links). Equating the coefficients of the simplified analytical polynomial with those of the prescribed characteristic polynomial derived from the pole allocation method yields the following system of nonlinear algebraic equations in the four unknowns (i.e., ω_1, f, μ, and ξ_2), as made explicit in what follows:

$$\begin{cases}
f\,\omega_1^4\,\mu^{-1} = \Omega_1^2\,\Omega_2^2 \\
\sqrt{f\,\mu^{-1}}\,\xi_2\,\omega_1^3 = \Omega_1\,\Omega_2\,(h_2\Omega_1 + h_1\Omega_2) \\
(1 + f + f\mu^{-1})\,\omega_1^2 = \Omega_1^2 + 4h_1h_2\Omega_1\Omega_2 + \Omega_2^2 \\
\left(\sqrt{f\,\mu^{-1}} + \sqrt{f\mu}\right)\xi_2\omega_1 = h_1\Omega_1 + h_2\Omega_2
\end{cases} \quad . \tag{11}$$

After defining the initial system of equations for pole allocation, the variables can be solved sequentially to express the design parameters in terms of target modal frequencies and damping ratios. Isolating the parameter f from the first Equation of Equation (11) yields

$$f = \frac{\mu\,\Omega_1^2\Omega_2^2}{\omega_1^4} \quad . \tag{12}$$

By substituting this expression for f into the second Equation of Equation (11) and applying the assumption $\omega_1 > 0$ along with positive physical constraints (i.e., $\mu > 0$, and all modal frequencies and damping ratios greater than 0), the target damping term ξ_2 can be derived as

$$\xi_2 = \frac{h_2\Omega_1 + h_1\Omega_2}{\omega_1} \quad , \tag{13}$$

being this expression an explicit function of the unknown natural frequency ω_1.

Finally, substituting the expressions for f and ξ_2 (Equations (12) and (13)) into the third equation of the system (Equation (11)) allows determining the mass ratio μ. Following algebraic simplification and assuming that all parameters are positive, the closed-form solution for μ can be obtained as

$$\mu = \frac{\omega_1^2(\Omega_1^2 + 4h_1h_2\Omega_1\Omega_2 + \Omega_2^2) - \omega_1^4 - \Omega_1^2\Omega_2^2}{\Omega_1^2\Omega_2^2} \quad . \tag{14}$$

The final stage of the symbolic derivation involves substituting the expressions for f, ξ_2, and μ (Equations (12), (13), and (14), respectively) into the fourth equation of the original system (Equation (11)). Following algebraic simplification assuming $\omega_1, \mu, \Omega_1, \Omega_2, h_1, h_2 > 0$ yields a governing equation that relates the design natural frequency ω_1 to the target poles.

$$\begin{aligned} &\frac{\Omega_1^2\Omega_2^2 + \left|\omega_1^4 + \Omega_1^2\Omega_2^2 - \omega_1^2\left(\Omega_1^2 + 4h_1h_2\Omega_1\Omega_2 + \Omega_2^2\right)\right|}{\omega_1^2\Omega_1\Omega_2} = \\ &= \frac{h_1\Omega_1 + h_2\Omega_2}{h_2\Omega_1 + h_1\Omega_2} \quad . \end{aligned} \tag{15}$$

Equation (15) is a fourth-order polynomial in ω_1^2. Accounting for the sign of the expression within the absolute value (positive and negative) splits the problem into two distinct fourth-order equations, yielding eight analytical solutions for ω_1 occurring in pairs of equal magnitude and opposite signs ($\pm\omega_{1,i}$). Discarding the zero root, which falls outside the valid domain of the equation, leaves three distinct positive solutions that are retained for this study.

All nonzero solutions for ω_1 as a function of the target modal parameters $(\Omega_1, \Omega_2, h_1, h_2)$ are provided in Appendix A. Substituting these solutions for ω_1 into the expressions for μ, TMD dampingξ_2, and f (Equations (12), (13), and (14), respectively) yields the target mechanical parameters. For brevity, the complete set of the expressions is reported in Appendix A.

Finally, to facilitate the formulation in subsequent sections, it is beneficial to make explicit the mechanical stiffness of the coupling device as k_2. The closed-form expression for stiffness k_2 derived via the pole allocation method is provided in the same subsection of Appendix A.

This systematic approach ensures that the physical parameters of the system can be precisely tuned to achieve the desired closed-loop poles. Selecting only the first solution for ω_1, manipulating the expressions of the stiffness, mass ratios, and damping ratio of the TMD, and noting that $\omega_2 = \omega_1\sqrt{f\mu^{-1}}$, the unified equation proposed in [33, 34, 35] can be recovered and provided in what follows

$$\frac{\xi_2}{\omega_2} = \left(\frac{h_1}{\Omega_1} + \frac{h_2}{\Omega_2}\right) \quad . \tag{16}$$

The dependence of the structural parameters on the poles and modal damping ratios indicates that the mechanical properties (f, ξ_2, ω_1, and μ) of the two DoFs can be obtained by prescribing a specific dynamic response, i.e., assigning Ω_1, Ω_2, h_1 and h_2.

Meanwhile, the explicit pole positions in the Gauss-plane and the corresponding modal damping ratios can be evaluated as functions of the input mechanical parameters by solving the system (Equation (11)) for the appropriate unknowns. This helps discuss the fluctuation, variance, and uncertainty of the TMD parameters. Within this perspective, ω_1, k_2, ξ_2, and μ serve as the known input parameters, while Ω_1, Ω_2, h_1, and h_2 represent the unknown variables.

To extract such parameters from the system of equations of the pole allocation method (11), the first equation is rewritten as

$$\Omega_2 = \frac{\omega_2\omega_1}{\Omega_1} \quad . \tag{17}$$

Substituting Equation (17) into the second and third equations of the system (Equation (11)) yields

$$\Omega_1^2 + 4h_1h_2\omega_2\omega_1 + \left(\frac{\omega_2\omega_1}{\Omega_1}\right)^2 = (1+\mu)\omega_2^2 + \omega_1^2 \quad , \tag{18}$$

$$h_2\Omega_1 + h_1\Omega_2 = \xi_2\omega_1 \quad . \tag{19}$$

Then, by coupling the fourth equation of Equation (11) with Equation (19) yields

$$\begin{bmatrix}\Omega_1 & \Omega_2\\ \Omega_2 & \Omega_1\end{bmatrix}\begin{bmatrix}h_1\\ h_2\end{bmatrix} = \begin{bmatrix}(1+\mu)\xi_2\omega_2\\ \xi_2\omega_1\end{bmatrix} \quad ,$$

$$\begin{bmatrix}h_1\\ h_2\end{bmatrix} = \frac{\xi_2\Omega_1}{\Omega_1^4 - \omega_2^2\omega_1^2}\begin{bmatrix}(1+\mu)\omega_2\Omega_1^2 - \omega_2\omega_1^2\\ -(1+\mu)\omega_2^2\omega_1 + \omega_1\Omega_1^2\end{bmatrix} \quad . \tag{20}$$

Finally, substituting Equation (20) into Equation (18) yields

$$\begin{aligned}&\Omega_1^4 - \{(1+\mu)\omega_2^2 + \omega_1^2\}\Omega_1^2 + \omega_2^2\omega_1^2 +\\ &+\left(\frac{2\xi_2\omega_2\omega_1\Omega_1}{\Omega_1^4 - \omega_2^2\omega_1^2}\right)^2\{(1+\mu)\Omega_1^2 - \omega_1^2\}\{\Omega_1^2 - (1+\mu)\omega_2^2\}\omega_2^2\omega_1^2 = 0 \quad .\end{aligned} \tag{21}$$

When the TMD is attached to the primary SDOF system, the natural circular frequencies ω_2, ω_1, Ω_1, and Ω_2 are close to each other. Consequently, because ξ_2^2 is smaller by orders of magnitude, the fourth term on the left side of the second row of Equation (21) becomes negligible, yielding

$$\Omega_1^4 - \{(1+\mu)\omega_2^2 + \omega_1^2\}\Omega_1^2 + \omega_2^2\omega_1^2 = 0 \quad . \tag{22}$$

The corresponding solution is

$$\begin{aligned}\Omega_1^2 &= \frac{(1+\mu)\omega_2^2 + \omega_1^2 \pm \sqrt{\{(1+\mu)\omega_2^2 + \omega_1^2\}^2 - 4\omega_2^2\omega_1^2}}{2}\\ &= \frac{(1+\mu)\omega_2^2 + \omega_1^2 \pm \sqrt{(1+\mu)^2\omega_2^4 + 2(1+\mu)\omega_2^2\omega_1^2 + \omega_1^4 - 4\omega_2^2\omega_1^2}}{2}\\ &= \frac{(1+\mu)\omega_2^2 + \omega_1^2 \pm \sqrt{(1+\mu)^2\omega_2^4 - 2(1-\mu)\omega_2^2\omega_1^2 + \omega_1^4}}{2} \quad .\end{aligned} \tag{23}$$

From the two solutions of Ω_1, both of which must be retained to not lose probability mass when performing the stochastic analyses, we can obtain Ω_2 via Equation (17), and h_1 and h_2 via Equation (20).

3. Effects of the randomness of constitutive parameters on the response of the optimal TMDs

As is well established in the literature and discussed in the Introduction, several deterministic optimization procedures can be used to tune the mechanical parameters of the absorber. For example, the well-known Den Hartog approach can optimize the absorber parameters to minimize the amplification factor of the primary system. Similarly, the pole allocation method can position the eigenvalues of the system at a specific part of the Gauss-plane to govern the overall dynamics in a prescribed manner. However, to the best of the authors' knowledge, despite input excitations frequently being referred to as random terms in the inherent literature, only a few studies have accounted for the stochastic variability of constitutive material parameters that often characterizes real-life structures when designing TMD systems. Neglecting this inherent randomness of the problem can lead to sub-optimal configurations, and consequently, to a significant de-tuning of the TMD system.

To evaluate the sensitivity of the system to variability in the absorber stiffness and damping parameters (i.e., k_2 and ξ_2), we analyze the dynamic response using the transfer functions, pole locations, and modal damping ratios derived through the pole allocation method. We consider the system in Equation (1) and subject it to ground motion at the base. To evaluate the poles, modal damping ratios, and amplification factors, the system parameters $(k_2, \xi_2, \mu, \omega_1)$ are specified, and then, the structural response is evaluated using Equations (17),(20), and (23).

The stochasticity of the absorber parameters is modeled using normal distributions as

$$p(k_2) = \frac{1}{\sqrt{2\pi\sigma_{k_2}^2}} \exp\left(-\frac{1}{2}\frac{(k_2 - \mu_{k_2})^2}{\sigma_{k_2}^2}\right) \quad , \tag{24}$$

$$p(\xi_2) = \frac{1}{\sqrt{2\pi\sigma_{\xi_2}^2}} \exp\left(-\frac{1}{2}\frac{(\xi_2 - \mu_{\xi_2})^2}{\sigma_{\xi_2}^2}\right) \quad , \tag{25}$$

where μ_{k_2} and μ_{ξ_2} represent the mean values of the absorber stiffness and damping ratio, respectively, and σ_{k_2} and σ_{ξ_2} arethe associated standard deviations. Assuming stochastic independence between the two random variables, the parameter pair (k_2, ξ_2) is sampled from their normal distributions. Hereafter, each generated pair is referred to as one realization and used to evaluate the response of the analyzed two-DoF system.

To demonstrate the limitations of relying on a deterministic approach to define optimal parameters, we deliberatelyselect the classic optimization procedure proposed by Den Hartog [1]. In this context, the mean values of the assumed distributions are considered equal to the optimal values obtained from Den Hartog's approach, as recalled in what follows:

$$\omega_{2,\mathrm{DH}}(\mu) = \frac{\omega_1}{1+\mu} \Rightarrow k_{2,\mathrm{DH}}(\mu) = \frac{m_1\,\mu\,\omega_1^2}{(1+\mu)^2} = \mu_{k_2} \quad , \tag{26}$$

$$\xi_{2,\mathrm{DH}}(\mu) = \sqrt{\frac{3\,\mu}{8(1+\mu)}} = \mu_{\xi_2} \quad . \tag{27}$$

For simplicity and illustrative purposes, stochasticity variability is restricted to the stiffness, while the damping ratio is assumed to be deterministic. Therefore, the standard deviation of stiffness k_2 is set to 20% of its mean value.

The analyses are performed by setting $\omega_1 = 2\pi$ rad/s and $\mu = 0.01$.

As demonstrated by the proposed relations, the pole allocation method governs the pole locations in the representative plane (Ω_1, Ω_2) by tuning the absorber parameters. These parameters are stochastic, and therefore, the resulting poles are spread across the pole-plane in a cloud of points. However, owing to the pole allocation equations that work as additional constraints linking Ω_2 with Ω_1 (Equation (17)), the poles must move along a specific fixed curve $\Omega_2 = \Omega_2(\Omega_1)$ in the same plane. Their equation can be obtained by solving Equation (22) for ω_2 and substituting the result into Equation (17), which yields

$$\Omega_2 = \omega_1 \sqrt{\frac{\Omega_1^2 - \omega_1^2}{\Omega_1^2(1+\mu) - \omega_1^2}} \quad . \tag{28}$$

Quite trivially, no sorting is *a priori* assumed for the two modes, and therefore, the interchangeability of Ω_1 and Ω_2 ensures that the two curves in Figure 2(a) are symmetric with respect to the plane bisector.

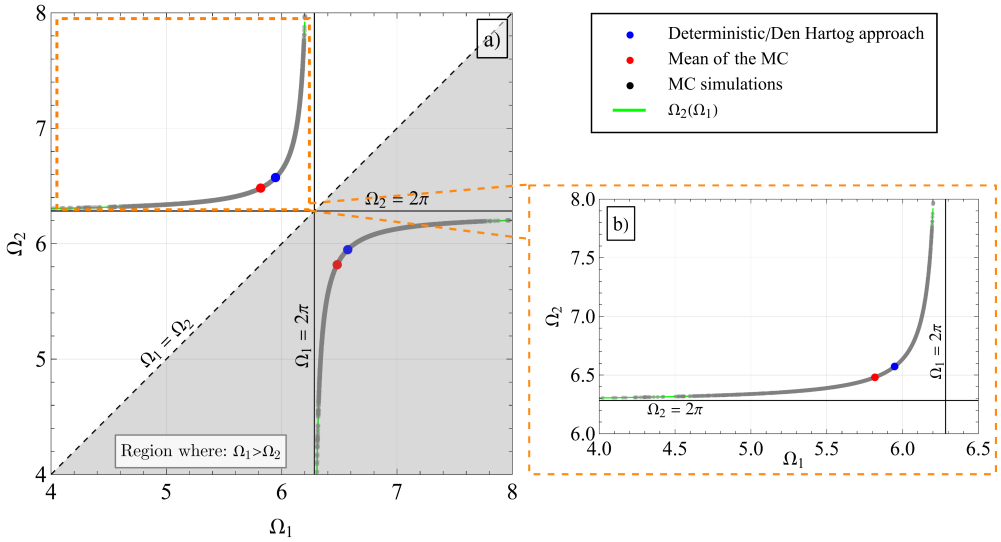


Figure 2: Pole localization in the (Ω_1, Ω_2) plane of the 2-DoF system considered in this study when $\mu_{k_2} = k_{2,\mathrm{DH}} = 851$ kN/m, $\sigma_{k_2} = 20\%\,\mu_{k_2}$, $\mu_{\xi_2} = \xi_{2,\mathrm{DH}} = 0.061, \mu_{\xi_2}, \mu = 0.01, m_1 = 2.2{\times}10^6$ kg, and $\sigma_{\xi_2} \to 0$. Given the random nature of the parameter k_2 of the absorber, the position of the poles in the plane also becomes random, i.e., the three thousand grey dots obtained through Monte Carlo (MC) simulations. All these realizations are located on a specific curve in the plane, in green. The mean response is represented by the red dot. In contrast, the blue dot represents the response of the system when choosing the average values of the parameter of the absorber. Given the arbitrariness of the pole cardinality introduced by the pole-allocation method, two symmetric solutions arise in the plane, wherein, only the solution belonging to the $\Omega_1 < \Omega_2$ half-plane region can be selected without losing the mass of probability.

Figure 3 illustrates the PDFs obtained from Monte Carlo (MC) simulations based on 3000 independent realizations. Although this sample size may be considered a relatively small, it provides an accurate agreement with the analytical results presented below.

The first row shows the distributions of the two poles, $(p(\Omega_i))$, whereas the second row presents those of the corresponding modal damping ratios, $(p(h_i))$.

Several inferences can be drawn from the shapes of these distributions. For the poles, panels (a) and (b) compare the stochastic mean of each distribution (red vertical line) with its corresponding deterministic value (blue vertical line). The deterministic values are obtained by setting the mechanical properties of the absorber equal to their mean values, which in the present analysis coincides with the optimal Den Hartog parameters.

For the first pole, the mean of the stochastic distribution is $\mathbb{E}[\Omega_1] = 5.82$ rad/s, whereas the deterministic analysis yields $\Omega_1 = 6.01$ rad/s, corresponding to a difference of approximately 3.2%. Similarly, the second pole exhibits a stochastic mean of $\mathbb{E}[\Omega_2] = 6.67$ rad/s compared to a deterministic value of $\Omega_2 = 6.50$ rad/s.

This discrepancy is a direct consequence of the nonlinear relationship between the uncertain input parameters (k_2, ξ_2) and the resulting modal quantities. As is well established, for a nonlinear function $Y = g(\mathbf{X})$,

$$\mathbb{E}[g(\mathbf{X})] \neq g\left(\mathbb{E}[\mathbf{X}]\right), \tag{29}$$

where $\mathbb{E}[\cdot]$ represents the expectation operator [36]. Consequently, a deterministic analysis performed using the mean values of the absorber properties does not necessarily predict the mean response of the stochastic system. From a physical perspective, this implies that the uncertainty in the mechanical parameters of the TMD systematically shifts its effective tuning, even when these parameters are centered on their optimal deterministic values. The magnitude of this shift depends on the input distributions and nonlinear coupling between the absorber properties and modal response. This observation provides a strong motivation for adopting a stochastic approach.

The horizontal dispersions of the pole distributions are quantified by their standard deviations $\sigma_{\Omega_1} = 0.14$ rad/s and $\sigma_{\Omega_2} = 0.10$ rad/s, which correspond to the coefficients of variation of approximately 2.4% and 1.5%, respectively.

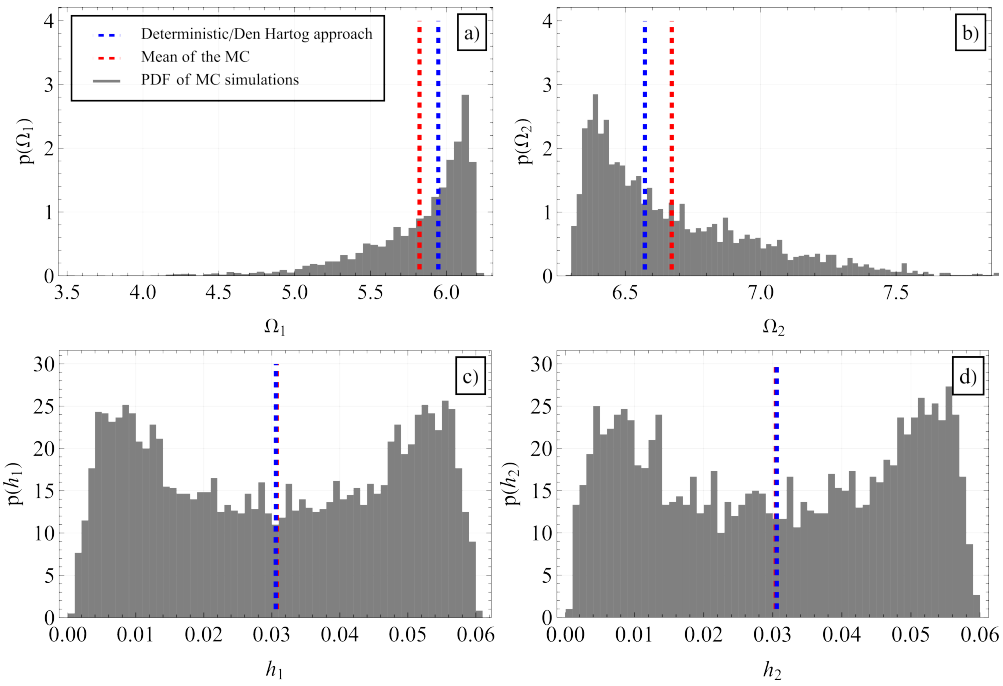


Figure 3: (Top row) PDFs of the poles (Ω_1, Ω_2), and (bottom row) modal damping ratios (h_1, h_2) obtained through MC simulations for $\mu_{k_2} = k_{2,\mathrm{DH}} = 851$ kN/m, $\sigma_{k_2} = 20\%\ \mu_{k_2}$, $\mu_{\xi_2} = \xi_{2,\mathrm{DH}} = 0.061$, $\mu = 0.01$, $m_1 = 2.2 \times 10^6$ kg, and $\sigma_{\xi_2} \to 0$. The means of the output distributions are indicated in red, whereas the deterministic responses evaluated using the mean input properties of the TMD, (ξ_2, k_2), are indicated in blue.

Although relatively small compared with the absolute values of the poles, these variations are still relevant when compared with the separation between the modal frequencies and with the tuning bandwidth of the absorber. Therefore, they indicate that uncertainty in the mechanical properties of the TMD propagates to the locations of the system poles.

The distributions are markedly asymmetric and characterized with skewness coefficients $\kappa_{\Omega_1} = -1.75$ and $\kappa_{\Omega_2} = +1.20$ [36]. The negative skewness of $p(\Omega_1)$ indicates a longer tail towards lower frequencies, whereas the positive skewness of $p(\Omega_2)$ indicates a longer tail toward higher frequencies. This asymmetry can be attributed to the nonlinear relationship between the uncertain mechanical parameters and system poles.

Although the *maxima* of the two marginal PDFs appear closer than the corresponding mean and deterministic values, their distance does not represent the most probable pole separation because the two marginal maxima do not necessarily occur within the same stochastic realization. A direct analysis of $\Delta\Omega = \Omega_2 - \Omega_1$ in Figure 4 indicates that all MC realizations exhibit a separation of the poles $(\Delta\Omega)$ greater than the deterministic value $(\Omega_{2,\mathrm{DH}} - \Omega_{1,\mathrm{DH}})$, and all gray realizations are on the right of the DH deterministic response in blue in the figure. Thus, any deviation from the optimal Den Hartog value induce a greater separation between the two poles.

Panels (c) and (d) show the bimodal distributions of the modal damping ratios, indicating the existence of two statistically preferred damping regimes. The mean values lie in comparatively less probable regions and therefore do not represent the most typical realizations of the system. Individual realizations are instead more likely to exhibit either a relatively low or a relatively high modal damping ratio.

This interpretation is confirmed by the empirical joint distribution of h_1 and h_2. The samples are strongly concentrated along the line, i.e.,

$$h_1 + h_2 \simeq \xi_2 = 0.061 \quad , \tag{30}$$

The two variables exhibit an almost perfectly negative correlation. Therefore, the overall amount of modal damping remains approximately constant, whereas its allocation between the two modes varies substantially. An increase in the damping ratio of one mode is accompanied by an almost equal reduction in that of the other.

The two solution branches are symmetric and exchange the roles of the modes: a realization characterized by the

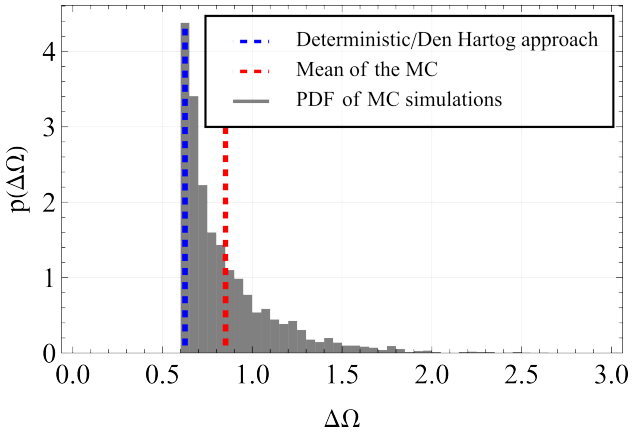


Figure 4: PDFs of the difference of the poles values ($\Delta\Omega = \Omega_2 - \Omega_2$) obtained through MC simulations for $\mu_{k_2} = k_{2,\mathrm{DH}} = 851$ kN/m, $\sigma_{k_2} = 20\%\ \mu_{k_2}$, $\mu_{\xi_2} = \xi_{2,\mathrm{DH}} = 0.061$, $\mu = 0.01$, $m_1 = 2.2{\times}10^6$ kg, and $\sigma_{\xi_2} \to 0$. The means of the output distributions are indicated in red, whereas the deterministic responses evaluated using the mean input properties of the TMD, (ξ_2, k_2), are indicated in blue.

pair (h_1, h_2) in one branch corresponds to the pair (h_2, h_1) in the other. The marginal modes (peaks) are located at approximately

$$h_{\mathrm{low}} \simeq 0.0087\ , \qquad h_{\mathrm{high}} \simeq 0.0525\ . \tag{31}$$

Thus, in the most probable configurations, the more strongly damped mode carries approximately 86% of the total modal damping, while the remaining 14% is associated with the other mode. Therefore, the stochastic response exhibits a preferential concentration of the available damping in one mode rather than an approximately equal sharing between the two modes. This behavior can be interpreted as a stochastic modal-damping separation with two branches identifying the two modes that receive the larger fraction of the available dissipation.

Moreover, we investigated the PDF of the expression ξ_2/ω_2, whose deterministic result has been made explicit in Equation (16), to grasp the relationship between the total available prescribed damping ξ_2 and modal dampings and poles. Similar to the other expressions, we implement MC simulations whose results are illustrated in Figure 5. The PDF of the ratio ξ_2/ω_2 is not perfectly symmetric and instead exhibits a noticeable positive skewness. Consequently, owing to this right-tailed distribution, the mean of the MC simulations (red dashed line) is slightly shifted towards higher values than the deterministic response based on the Den Hartog approach (blue dashed line). This discrepancy demonstrates that evaluating the system in a purely deterministic manner, i.e., by exclusively employing the mean input properties of the TMD set following the Den Hartog approach, leads to a slight underestimation of the expected average response compared to that of a comprehensive probabilistic assessment.

Finally, the histogram illustrates a broad dispersion of the output ratio, with values ranging from 0.0075 to over 0.013. This considerable variance underscores the significant impact that the introduced mechanical uncertainties, such as the 20% standard deviation associated with the stiffness parameter k_2, exert on the overall dynamic response of the system.

In Figure 6, the deterministic amplification factors of the two DoFs are compared with those obtained by accounting for stochasticity.

The grey curves in Figure 6 are obtained through MC simulations, wherein absorber parameters are generated randomly from normal probability distributions, and the mechanical response of the entire structure is evaluated for each realization.

Further, the red curves represent the mean responses of the grey MC realizations obtained by taking their arithmetic average. Thus, they describe the mean stochastic amplification factors.

In contrast, the blue curves represent the amplification factors of the two degrees of freedom when the mechanical parameters are set equal to their optimal Den Hartog mean values. As is clearly evident, the difference between the red and blue curves is straightforward.

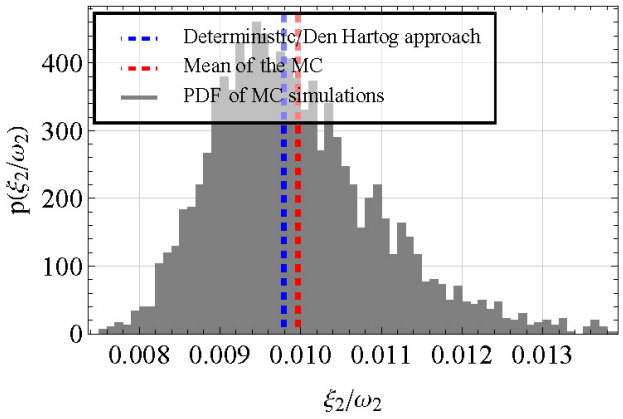


Figure 5: PDFs of the ratio ξ_2/ω_2 obtained through MC simulations for $\mu_{k_2} = k_{2,\mathrm{DH}} = 851$ kN/m, $\sigma_{k_2} = 20\%\ \mu_{k_2}$, $\mu_{\xi_2} = \xi_{2,\mathrm{DH}} = 0.061$, $\mu = 0.01$, $m_1 = 2.2 \times 10^6$ kg, and $\sigma_{\xi_2} \to 0$. The means of the output distributions are indicated in red, whereas the deterministic responses evaluated using the mean input properties of the TMD, (ξ_2, k_2), are indicated in blue.

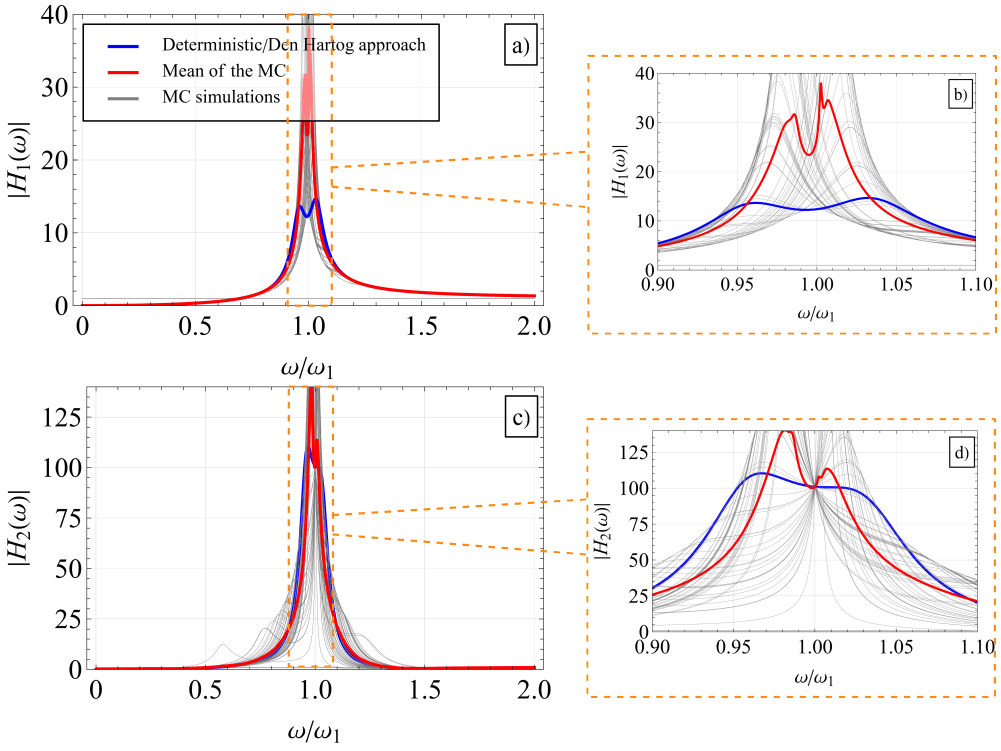


Figure 6: Amplification factors for the analyzed two-DoF system described by Eqs. (1) for the first mass (up) and second mass (below). The mechanical parameters are set as follows: $\omega_1 = 2\pi$ rad/s, $m_1 = 2.2 \times 10^6$ kg, $\mu = 0.01$, $\mu_{k_2} = 851.4$ kN/m, $\mu_{\xi_2} = 0.061$, $\sigma_{k_2} = 20\%\ \mu_{k_2}$, and $\sigma_{\xi_2} \to 0$. To avoid excessive overlapping of the curves and consequent difficulty in reading each response, only one hundred realizations of the three thousand available computed in the MC procedure are shown; each individual result is shown in grey. The red curve represents the average response over all stochastic simulations, while the blue curve denotes the deterministic response obtained using the mean values of the normal distributions as input mechanical parameters, which is thus the desired optimal configuration. The graphs therefore compare the average stochastic response with the response associated with the average parameter values, highlighting the differences between the two.

4. Incorporating uncertainties into pole allocation method

Although the previous section provided closed-form solutions for the design variables based on the pole allocation technique, it assumed that all mechanical properties were perfectly deterministic. In practical engineering applications, devices such as seismic isolators, dampers, or springs that couple the primary mass to the secondary mass exhibit intrinsic variability that stems from manufacturing tolerances, environmental conditions (such as temperature fluctuations affecting oil viscosity in dampers), material fatigue over time, or even empirical deviations of measurements. The stiffness and equivalent linearized damping of these connecting devices (i.e., k_2 and ξ_2 in the idealized scheme of Figure 1) are subject to uncertainty, and the actual performance of the system may deviate from the target deterministic poles (Ω_i, h_i).

To address this issue and evaluate the effects of this variability on the response of the system, it is necessary to incorporate this randomness into the selected optimization methodology.

To account for the inherent uncertainties in the mechanical problem, the equivalent stiffness k_2 and damping ratio ξ_2 are modelled as independent random variables, each following one Gaussian (normal) distribution (24) and (25). In this stochastic framework, μ_{k2}, μ_{ξ_2} and $\sigma_{k2}, \sigma_{\xi_2}$ are referred to as the mean and variance values of k_2 and ξ_2, respectively, and they are provided by the manufacturer.

Without loss of generality, the joint PDF for the system parameters is obtained by assuming statistical independence between the stiffness and damping variations as the product of the individual marginal distributions.

$$p(k_2, \xi_2) = p(k_2) \cdot p(\xi_2) \quad . \tag{32}$$

The probability distribution of the poles Ω_1 and Ω_2 following the pole allocation method can be evaluated by invoking the well-known theorem of transformation of random variables [37, 36], as provided in the following:.

$$p(\Omega_1, \Omega_2) = \frac{|\det \mathbf{J}|}{2\pi\sigma_{k_2}\sigma_{\xi_2}} \exp\left\{-\frac{1}{2}\left[\left(\frac{k_2 - \mu_{k_2}}{\sigma_{k_2}}\right)^2 + \left(\frac{\xi_2 - \mu_{\xi_2}}{\sigma_{\xi_2}}\right)^2\right]\right\} \quad , \tag{33}$$

where $\det \mathbf{J}$ represents the determinant of the Jacobian matrix $\mathbf{J}$, while $k_2 = k_2(\Omega_1, \Omega_2)$ and $\xi_2 = \xi_2(\Omega_1, \Omega_2)$.

When the inverse transformation is not unique (i.e., $\Omega_i = \Omega_i(k_2, \xi_2)$) as a consequence of the nonlinearity of the system in Equation (11), all admissible inverse branches must be retained in the change-of-variables formula. A given pair (Ω_1, Ω_2) may correspond to several distinct points in the original random-variable space. Neglecting any of these preimages would omit its contribution to the transformed density and result in a loss of probability mass [36]. For the present problem, the nonlinear inverse mapping admits three distinct positive solutions for ω_1 for a given pair (Ω_1, Ω_2), namely, those of Equation (15). Consequently, three solutions arise for μ from Equation (14), and thus, three corresponding pairs

$$\left(k_2^{(i)}, \xi_2^{(i)}\right), \qquad i = 1, 2, 3, \tag{34}$$

are obtained from Equations (12) and (13). The joint PDF of (Ω_1, Ω_2) must therefore be evaluated by summing the contributions associated with all three inverse branches.

$$p(\Omega_1, \Omega_2) = \sum_{i=1}^{3} \frac{\left|\det \mathbf{J}^{(i)}\right|}{2\pi\sigma_{k_2}\sigma_{\xi_2}} \exp\left\{-\frac{1}{2}\left[\left(\frac{k_2^{(i)} - \mu_{k_2}}{\sigma_{k_2}}\right)^2 + \left(\frac{\xi_2^{(i)} - \mu_{\xi_2}}{\sigma_{\xi_2}}\right)^2\right]\right\} \quad , \tag{35}$$

where $\mathbf{J}^{(i)}$ represents the Jacobian matrix of the inverse transformation evaluated along the ith branch. The explicit expressions for the three solutions $k_2^{(i)}$ and $\xi_2^{(i)}$ are reported in Appendix A.

The Jacobian matrix evaluates the transformation of the parameters $k_2(\Omega_1, \Omega_2)$ and $\xi_2(\Omega_1, \Omega_1)$ with respect to the modal frequencies, and it is defined as

$$\mathbf{J}^{(i)} = \begin{bmatrix} \dfrac{\partial k_2^{(i)}}{\partial \Omega_1} & \dfrac{\partial k_2^{(i)}}{\partial \Omega_2} \\ \dfrac{\partial \xi_2^{(i)}}{\partial \Omega_1} & \dfrac{\partial \xi_2^{(i)}}{\partial \Omega_2} \end{bmatrix} \quad , \tag{36}$$

where the symbol ∂ represents the partial derivative with respect to the specified modal frequency variables, i.e., Ω_1 and Ω_2.

The new PDF (35) is obtained by employing the well-known theorem of transformation of random variables. When the cumulative distribution function (CDF) approaches 1, the integration domain is the half space defined by $\Omega_1 \in (-\infty, +\infty)$ while $\Omega_2 > \Omega_1$ (see Figure 2), i.e.,

$$\int_{-\infty}^{+\infty} \int_{\Omega_1}^{+\infty} p(\Omega_1, \Omega_2)\, d\Omega_2\, d\Omega_1 = 1 \quad . \tag{37}$$

A numerical representation of the PDF $p(\Omega_1, \Omega_2)$ is illustrated in Figure 7 for two different set of values for the modal dampings, $h_1 = h_2$ on the left column, and $h_1 > h_2$ on the right column.

As depicted in the 3D surface plot (Figure 7a) or d), the joint PDF is concentrated along a single ridge. The target values of the present analysis are the two poles (Ω_i) and modal damping ratios (h_i). Thus, these four parameters are considered independent variables. To visualize the position of the poles in the plane and their PDFs, the target modal dampings must be assigned.

The two-dimensional(2D) cross-sections presented in Figures 7b and 7c for the $h_1 = h_2$ case, or d) and e) for the unequal case $h_1 > h_2$ provide a clear view of the local behavior. The resulting profiles clearly highlight the nature of response that is slightly Gaussian-like by slicing the 3D surface at constant frequencies ($\Omega_1 = 5.95$ rad/s and $\Omega_2 = 6.57$ rad/s, respectively). In both sections, the distribution approaches 0 around the intersection point ($\Omega_1 = \Omega_2$), confirming that the joint probability vanishes when the two eigenvalues are the same. This result can be attributed to the decoupling of two modal responses prescribed by the pole allocation method, as provided by Equation (8). In fact, the first and second modes are exchangeable in Equation (8) because no mathematical sorting is *a priori* prescribed to the eigenvalues or modal frequencies.

The different scales used in panels (b) and (c) of Figure 7, compared with those in panels (e) and (f), can be attributed to the different target modal damping ratios ($h_1 \neq h_2$). Under this condition, realizations close to $(\Omega_1, \Omega_2) = (5.95, 6.57)$, rad/s are significantly less likely than when the target modal damping ratios are comparable.

Finally, quantitative comparisons between the illustrative numerical approach presented in Section 3 and the analytical procedure outlined in the present section are outlined in Appendix B, where an easy-to-implement algorithm is outlined and explained in detail.

5. Conclusions

This work presented an analytical framework for incorporating uncertainties in the mechanical parameters of the absorber into the pole allocation design of passive TMDs. In contrast to standard deterministic procedures, the proposed approach treats them as random variables and evaluates how their variability propagates to the poles and modal damping ratios of the coupled system, affecting their optimal design.

The analytical formulation based on the theorem of transformation of random variables provides a closed-form joint PDF of the system poles and modal dampings. Owing to the nonunique nature of the inverse transformation between poles and absorber parameters, all admissible branches must be retained to avoid any loss of probability mass for the PDFs of the poles. This indicates a key aspect of the proposed methodology and enables the stochastic pole allocation problem to be treated with mathematical consistency. This analytical setup is tested against numerical simulations relying on a MC approach.

The following conclusions are drawn from the results. The plots indicate that the response obtained using the mean values of the absorber parameters do not coincide with the mean stochastic response. This discrepancy is a direct consequence of the nonlinear relationship between the physical properties of the TMD and modal quantities of the system. Such an effect implies that even when the absorber parameters are centered around their deterministic optimal values, the design goal and its intrinsic uncertainty may induce a systematic shift in the pole locations and modal dampings, consequently de-tuning the device.

Both MC simulations and the analytical stochastic framework indicate that the poles are not scattered arbitrarily in the frequency plane; however, they remain constrained along specific curves dictated by the pole allocation equations, which works as a constraint on the position of the values available for the poles. The resulting probability distributions are asymmetric and show a marked tendency to shift poles apart (higher chance a fluctuation in the absorber parameters

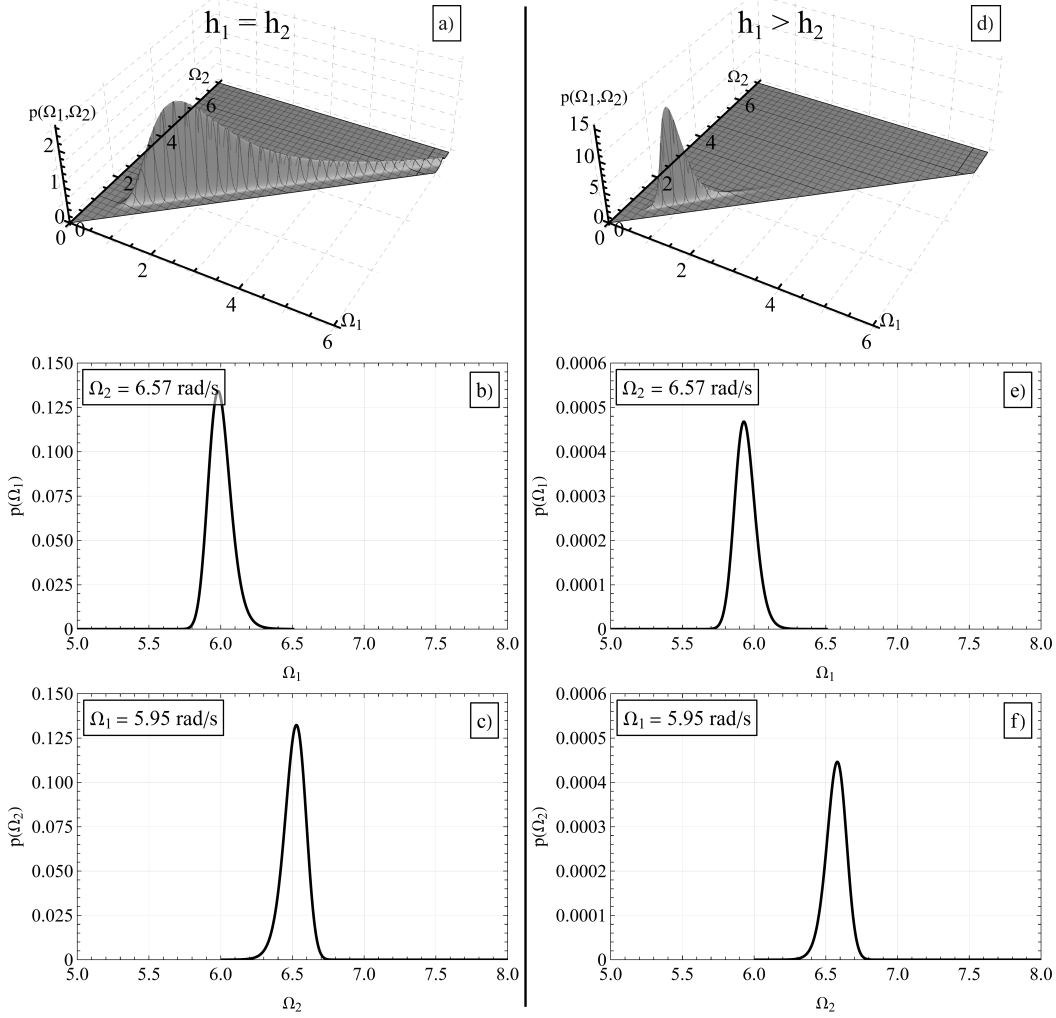


Figure 7: Joint PDFs $p(\Omega_1, \Omega_2)$ of modal frequencies Ω_1 and Ω_2, with the right hand indicating the case where $h_1 > h_2$ and the left side being referred to $h_1 = h_2$. Subplots (a) and (d) report 3D surface representations of the joint PDF in the two above-mentioned configurations, while the subpanels (b), (c), (e), and (f) provide the 2D relative cross-section evaluated at constant frequency $\Omega_2 = 6.57$ rad/s and $\Omega_1 = 5.95$ rad/s. All the numerical simulations in this figure are performed using the following parameter set: $\mu_{k_2} = k_{2,\mathrm{DH}} = 851$ kN/m, $\sigma_{k_2} = 20\%\,\mu_{k_2}$, $\mu_{\xi_2} = \xi_{2,\mathrm{DH}} = 0.061$, $\sigma_{\xi_2} = 5\%\,\mu_{\xi_2}$, $\mu = 0.01$, and $m_1 = 2.2 \times 10^6$ kg. For the left column, the modal damping ratios are prescribed as $h_1 = h_2 = 0.031$, while on the right side, $h_2 = 0.02$.

strengthens modal separation). In contrast, modal damping ratios may exhibit bimodal behavior, indicating that the available damping is not necessarily shared equally between the two modes. Instead, the stochastic response tends to favor configurations in which one mode receives most of the dissipation, while the other remains weakly damped.

Overall, the study demonstrates that accounting for uncertainties in the absorber stiffness and damping is essential for performing a more realistic assessment of TMD performance and properly designing these devices. The proposed framework offers a rigorous basis for moving from deterministic tuning rules towards more robust design strategies, where not only the nominal pole locations but also their probability distribution can be *ad hoc* controlled. Finally, the broader implications and societal impact of the study findings have been highlighted in order to demonstrate how the provided methodology advances resilient structural control, thereby enhancing the safety and longevity of civil infrastructure against extreme environmental hazards.

Future developments may extend the approach to more general uncertainty models, such as non-Gaussian distributions to account for skewed manufacturing tolerances or time-dependent material degradation, and scale the framework to complex multi-DOF structures. Furthermore, future efforts will aim to address current methodological limitations, including the assumption of statistical independence between mechanical parameters and the restriction to linear structural systems.

Acknowledgements

M.A. acknowledges the support from "SiciliAn MicronanOTecH Research And Innovation CEnter 'SAMOTHRACE" (MUR, PNRR-M4C2, ECS_00000022), spoke 3 – University of Palermo "S2-COMMs – Micro and Nanotechnologies for Smart & Sustainable Communities". R.C. acknowledges the support of the Italian Ministry of University and Research through grant FIT4MEDROB (PNC0000007).

Author contributions

M.A.: Conceptualization, Methodology, Software, Validation, Formal analysis, Investigation, Data curation, Writing - Original draft, Review and editing, and Visualization. R.C.: Conceptualization, Methodology, Software, Validation, Formal analysis, Investigation, Data curation, Writing - Original draft, Review and editing, and Visualization. Y.I.: Conceptualization, Methodology, Formal analysis, Investigation, Writing - Review and editing, Supervision.

Conflicts of Interest

The authors declare no conflicts of interest.

Appendix A. Pole allocation analytical solutions

The complete set of solutions for Equation (15) is presented excluding the root $\omega_1 = 0$ with algebraic multiplicity 2, which allows evaluating the entire group of other mechanical parameters involved in the two DoFs investigated in this study. Therefore, from the 8 distinct solutions theoretically derived from the two different 4-th order Equations (15), the following 6 are reported here. For the sake of clarity and ease of understanding, a series of coefficients are defined first.

$$\begin{aligned}
S &= h_2\Omega_1 + h_1\Omega_2 \quad , \\
T &= h_1\Omega_1 + h_2\Omega_2 \quad , \\
C &= \Omega_1^2 + \Omega_2^2 + 4h_1h_2\Omega_1\Omega_2 \quad , \\
P &= SC - \Omega_1\Omega_2 T \quad , \\
N &= \left(\Omega_1^2 - \Omega_2^2\right)^2 + 4\Omega_1\Omega_2 ST \quad , \\
\Delta &= (P + 2\Omega_1\Omega_2 T)^2 - 8\Omega_1^2\Omega_2^2 S^2, \\
R &= P - 2\Omega_1\Omega_2 T \quad ,
\end{aligned} \tag{A.1}$$

All of these coefficients are functions of the modal parameters $\Omega_{1,2}$ and $h_{1,2}$. Accordingly, ω_1 reads

$$\begin{aligned}
\omega_{1,1} &= \sqrt{\frac{P}{S}} \quad , \\
\omega_{1,2} &= \sqrt{\frac{P + 2\Omega_1\Omega_2 T - \sqrt{\Delta}}{2S}} \quad , \\
\omega_{1,3} &= \sqrt{\frac{P + 2\Omega_1\Omega_2 T + \sqrt{\Delta}}{2S}} \quad .
\end{aligned} \tag{A.2}$$

Among the six solutions for ω_1, the roots preceded by a minus sign are trivially negative and can be immediately discarded, retaining only the positive ones (There are only three such solutions).

Through Equation (14), we obtain roots for the mass ratio μ, namely,

$$\mu_1 = \frac{h_1h_2N}{\Omega_1\Omega_2S^2} \quad , \tag{A.3}$$

$$\mu_2 = \frac{2\Omega_1\Omega_2S^2 - T\left(P + 2\Omega_1\Omega_2T\right) + T\sqrt{\Delta}}{2\Omega_1\Omega_2S^2} \quad , \tag{A.4}$$

$$\mu_3 = \frac{2\Omega_1\Omega_2S^2 - T\left(P + 2\Omega_1\Omega_2T\right) - T\sqrt{\Delta}}{2\Omega_1\Omega_2S^2} \quad . \tag{A.5}$$

Likewise, Equation (13) provides the damping ratio ξ_2.

$$\xi_{2,1} = \sqrt{\frac{S^3}{P}} \quad , \tag{A.6}$$

$$\xi_{2,2} = \frac{\sqrt{S\left(P + 2\Omega_1\Omega_2T + \sqrt{\Delta}\right)}}{2\Omega_1\Omega_2} \quad , \tag{A.7}$$

$$\xi_{2,3} = \frac{\sqrt{S\left(P + 2\Omega_1\Omega_2T - \sqrt{\Delta}\right)}}{2\Omega_1\Omega_2} \quad . \tag{A.8}$$

Equation (12) yields the stiffness ratio

$$f_1 = \frac{h_1 h_2 \Omega_1 \Omega_2 N}{P^2} \quad , \tag{A.9}$$

$$f_2 = \frac{2\Omega_1\Omega_2 \left[2\Omega_1\Omega_2 S^2 - T\left(P + 2\Omega_1\Omega_2 T\right) + T\sqrt{\Delta}\right]}{\left(P + 2\Omega_1\Omega_2 T - \sqrt{\Delta}\right)^2} \quad , \tag{A.10}$$

$$f_3 = \frac{2\Omega_1\Omega_2 \left[2\Omega_1\Omega_2 S^2 - T\left(P + 2\Omega_1\Omega_2 T\right) - T\sqrt{\Delta}\right]}{\left(P + 2\Omega_1\Omega_2 T + \sqrt{\Delta}\right)^2} \quad , \tag{A.11}$$

which corresponds to k_2.

$$k_{2,1} = \frac{m_1 h_1 h_2 \Omega_1 \Omega_2 N}{S P} \quad , \tag{A.12}$$

$$k_{2,2} = \frac{m_1}{4S}\left(R + \sqrt{\Delta}\right) \quad , \tag{A.13}$$

$$k_{2,3} = \frac{m_1}{4S}\left(R - \sqrt{\Delta}\right) \quad . \tag{A.14}$$

Appendix B. Probability density function of the system poles

To compare the analytical approach with the numerical results obtained in Section 3, the system (11) is solved for the set (f, ξ_2, h_1, h_2) with the quantities $(\Omega_1, \Omega_2, \mu, \omega_1)$ used as independent variables.

The two poles are assumed to be real, positive, and ordered according to $0 < \Omega_1 < \Omega_2$.

For convenience, we define

$$\Delta = \omega_1^4 - \omega_1^2\left(\Omega_1^2 + \Omega_2^2\right) + (1+\mu)\Omega_1^2\Omega_2^2 \quad . \tag{B.1}$$

Then, solving Equations (11) with respect to f, h_1, h_2, and ξ_2 yields

$$f = \frac{\mu\Omega_1^2\Omega_2^2}{\omega_1^4} \quad , \tag{B.2}$$

$$h_1 = \frac{1}{2\Omega_1\omega_1}\sqrt{\frac{\Delta\left[\omega_1^2 - (1+\mu)\Omega_1^2\right]}{(1+\mu)\Omega_2^2 - \omega_1^2}} \quad , \tag{B.3}$$

$$h_2 = \frac{1}{2\Omega_2\omega_1}\sqrt{\frac{\Delta\left[(1+\mu)\Omega_2^2 - \omega_1^2\right]}{\omega_1^2 - (1+\mu)\Omega_1^2}} \quad , \tag{B.4}$$

$$\xi_2 = \frac{\left(\Omega_2^2 - \Omega_1^2\right)\sqrt{\Delta}}{2\Omega_1\Omega_2\sqrt{\left[\omega_1^2 - (1+\mu)\Omega_1^2\right]\left[(1+\mu)\Omega_2^2 - \omega_1^2\right]}} \quad . \tag{B.5}$$

We retain only the positive branch of ξ_2 for physical consistency. The negative branch is disregarded as it corresponds to a different dynamical system. To invert Equation (B.5) with respect to Ω_2, the equation is first squared, which yields

$$\xi_2^2 = \frac{\left(\Omega_2^2 - \Omega_1^2\right)^2\left[\omega_1^4 - \omega_1^2\left(\Omega_1^2 + \Omega_2^2\right) + (1+\mu)\Omega_1^2\Omega_2^2\right]}{4\Omega_1^2\Omega_2^2\left[\omega_1^2 - (1+\mu)\Omega_1^2\right]\left[(1+\mu)\Omega_2^2 - \omega_1^2\right]} \quad . \tag{B.6}$$

After rearrangement, Equation (B.6) can be written as a cubic polynomial in Ω_2^2 as

$$a_3\Omega_2^6 + a_2\Omega_2^4 + a_1\Omega_2^2 + a_0 = 0 \quad , \tag{B.7}$$

where

$$\begin{aligned} a_3 &= (1+\mu)\Omega_1^2 - \omega_1^2 \quad , \\ a_2 &= \omega_1^4 + \Omega_1^2\omega_1^2 - 2(1+\mu)\Omega_1^4 + 4(1+\mu)\Omega_1^2\xi_2^2\left[(1+\mu)\Omega_1^2 - \omega_1^2\right] \quad , \\ a_1 &= \Omega_1^2\left\{(1+\mu)\Omega_1^4 + \Omega_1^2\omega_1^2 - 2\omega_1^4 + 4\omega_1^2\xi_2^2\left[\omega_1^2 - (1+\mu)\Omega_1^2\right]\right\} \quad , \\ a_0 &= \Omega_1^4\omega_1^2\left(\omega_1^2 - \Omega_1^2\right) \quad . \end{aligned} \tag{B.8}$$

Equation (B.7) is a sixth-order polynomial in Ω_2, and as such, it holds six roots (three positive and three negative, i.e., they are physically inconsistent) because the equation only presents the even terms in Ω_2^2. The three admissible solutions are denoted by

$$\left(\Omega_2^{(j)}\right)^2, \qquad j = 1, 2, 3. \tag{B.9}$$

In the non-degenerate case $a_3 \neq 0$, the three algebraic solutions for Ω_2^2 are

$$\left(\Omega_2^{(j)}\right)^2 = -\frac{1}{3a_3}\left[a_2 + \zeta_j C + \frac{\mathcal{D}_0}{\zeta_j C}\right], \qquad j = 1, 2, 3, \tag{B.10}$$

where one made use of the Cardano quantities defined as

$$\begin{aligned} \zeta_j &= \exp\left[\frac{2\pi i\,(j-1)}{3}\right] \quad , \\ \mathcal{D}_0 &= a_2^2 - 3a_3a_1 \quad , \\ \mathcal{D}_1 &= 2a_2^3 - 9a_3a_2a_1 + 27a_3^2a_0 \quad , \\ C &= \sqrt[3]{\frac{\mathcal{D}_1 + \sqrt{\mathcal{D}_1^2 - 4\mathcal{D}_0^3}}{2}} \quad . \end{aligned} \tag{B.11}$$

Equation (B.10) was obtained by squaring Equation (B.5), and therefore, the three algebraic branches are not necessarily all physically admissible. For each j, the branch is retained only if

$$\left(\Omega_2^{(j)}\right)^2 \in \mathbb{R}_+ \quad , \tag{B.12}$$

$$\Omega_2^{(j)} > \Omega_1 \quad , \tag{B.13}$$

and if substitution into the original non-squared Equation (B.5) returns the prescribed positive value of ξ_2. In the degenerate case $a_3 = 0$, Equation (B.7) reduces to a quadratic polynomial in Ω_2^2 and must be solved separately.

Branches of k_2. From Equation (B.2), the stiffness of the second oscillator is related to f by

$$k_2 = fm_1\omega_1^2 = \frac{m_1\mu}{\omega_1^2}\Omega_1^2\Omega_2^2 \quad . \tag{B.14}$$

Substitution of the three roots $\left(\Omega_2^{(j)}\right)^2$ yields the three inverse branches $k_2^{(j)}(\Omega_1)$, where $j = 1, 2, 3$.

Let I_j represent the interval in which the j-th branch is real, physically admissible, and monotonic, which implies some of the sets I_j may be empty, and therefore, not all three algebraic roots are necessarily physical. Furthermore, let k_2 represent the only uncertain system parameter, with a probability density function

$$k_2 \sim p_{k_2}(k_2) = \frac{1}{\sqrt{2\pi}\sigma_{k_2}} \exp\left[-\frac{(k_2-\mu_{k_2})^2}{2\sigma_{k_2}^2}\right] \quad , \tag{B.15}$$

For simplicity, this PDF is assumed to behave as a Gaussian distribution of average value μ_{k_2} and standard deviation σ_{k_2}.

The theorem of transformation of variables ensures the conservation of probability density states that the marginal probability distribution reads

$$p_{\Omega_1}(\Omega_1) = \sum_{j=1}^{3} \mathbf{1}_{I_j}\, p_{k_2}\left(k_2^{(j)}(\Omega_1)\right)\left|\frac{\mathrm{d}k_2^{(j)}}{\mathrm{d}\Omega_1}\right| \quad . \tag{B.16}$$

Here, $\mathbf{1}_{I_j}$ represents the indicator function of the admissibleinterval I_j that allows a branch to contribute only where real, physical, and consistent with the original positive-ξ_2 equation.

The same procedure can be followed to obtain the PDF of the second pole Ω_2 instead of the PDF of the first pole by solving the ξ_2 equation in Ω_1 and plugging the results into $k_2(\Omega_2)$, which then allows using the theorem applied above.

Joint probability distribution of the two poles. Starting from the two deterministic mappings (B.5) and (B.14), k_2 is random but ξ_2 is prescribed deterministically, and therefore, the joint distribution of (Ω_1, Ω_2) is concentrated on the curve

$$g(\Omega_1, \Omega_2) = \xi_2 \quad . \tag{B.17}$$

Consequently, the two poles do not possess an ordinary two-dimensional PDF with respect to the area measure $\mathrm{d}\Omega_1\,\mathrm{d}\Omega_2$, and thus, their generalized joint density can be written as

$$p_{\Omega_1,\Omega_2}(\Omega_1, \Omega_2) = \sum_{j=1}^{3} \mathbf{1}_{I_j} p_{k_2}\left(k_2^{(j)}(\Omega_1)\right)\left|\frac{\mathrm{d}k_2^{(j)}}{\mathrm{d}\Omega_1}\right| \delta\left[\Omega_2 - \Omega_2^{(j)}(\omega_1)\right] \quad , \tag{B.18}$$

where δ represents the delta Dirac distribution. The integration of the joint density with respect to the second pole recovers the marginal PDF of the first pole.

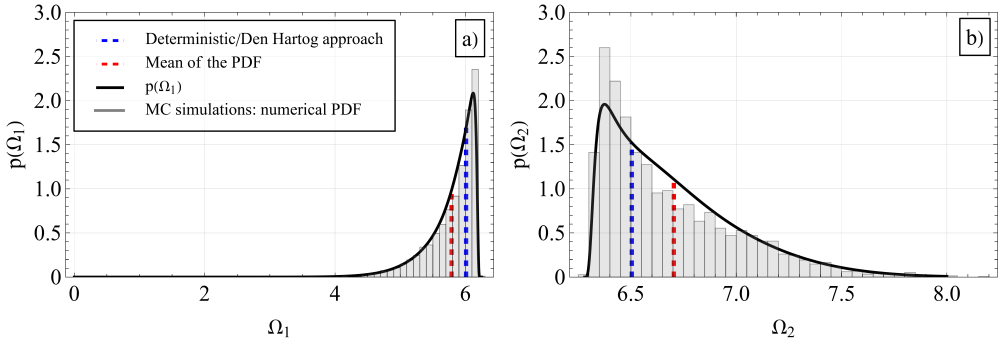


Figure B.8: PDF of the two poles (Ω_1 on the left and Ω_2 on the right) obtained from the analytical procedure presented (in black) versus numerical simulations using MC realizations (in grey). Mechanical parameters are set as $\omega_1 = 2\pi$ rad/s, $m_1 = 2.2 \times 10^6$ kg, $\mu = 0.01$, $\mu_{k_2} = 851.4$ kN/m, $\mu_{\xi_2} = 0.061$, $\sigma_{k_2} = 20\%\ \mu_{k_2}$, and $\sigma_{\xi_2} \to 0$. The numerical simulations are precisely those obtained in Figure 3.

References

[1] J. P. Den Hartog, Mechanical vibrations, Courier Corporation, 1985.

[2] S. Krenk, Frequency analysis of the tuned mass damper, Journal of Applied Mechanics 72 (6) (2005) 936–942.

[3] S. Krenk, J. Høgsberg, Tuned mass absorbers on damped structures under random load, Probabilistic Engineering Mechanics 23 (4) (2008) 408–415.

[4] H. Fang, L. Liu, D. Zhang, M. Wen, Tuned mass damper on a damped structure, Structural Control and Health Monitoring 26 (3) (2019) e2324.

[5] M. Argenziano, D. Faiella, A. Carotenuto, E. Mele, M. Fraldi, Generalization of the Den Hartog model and rule-of-thumb formulas for optimal tuned mass dampers, Journal of Sound and Vibration 538 (2022) 117213.

[6] M. Argenziano, A. Palmeri, A. R. Carotenuto, E. Mele, M. Fraldi, Optimization of viscoelastic tuned mass damper systems subjected to coloured excitations, Earthquake Engineering & Structural Dynamics 54 (12) (2025) 3244–3264.

[7] H. Frahm, Device for damping vibrations of bodies, US Patent No. 989,958, filed 30 October 1909; granted 18 April 1911 (1911).

[8] T. Ioi, K. Ikeda, On the dynamic vibration damped absorber of the vibration system, Bulletin of JSME 21 (151) (1978) 64–71.

[9] S. Randall, D. Halsted III, D. Taylor, Optimum vibration absorbers for linear damped systems, Journal of Mechanical Design 103 (4) (1981) 908–913.

[10] G. Warburton, Optimum absorber parameters for various combinations of response and excitation parameters, Earthquake Engineering & Structural Dynamics 10 (3) (1982) 381–401.

[11] H.-C. Tsai, G.-C. Lin, Optimum tuned-mass dampers for minimizing steady-state response of support-excited and damped systems, Earthquake engineering & structural dynamics 22 (11) (1993) 957–973.

[12] R. Villaverde, Reduction seismic response with heavily-damped vibration absorbers, Earthquake Engineering & Structural Dynamics 13 (1) (1985) 33–42.

[13] F. Sadek, B. Mohraz, A. W. Taylor, R. M. Chung, A method of estimating the parameters of tuned mass dampers for seismic applications, Earthquake Engineering & Structural Dynamics 26 (6) (1997) 617–635.

[14] C. Moutinho, An alternative methodology for designing tuned mass dampers to reduce seismic vibrations in building structures, Earthquake Engineering & Structural Dynamics 41 (14) (2012) 2059–2073.

[15] O. Lavan, Multi-objective optimal design of tuned mass dampers, Structural Control and Health Monitoring 24 (11) (2017) e2008.

[16] M. Yahyai, L. Zebarjad, M. Head, M. Shokouhian, Toward optimizing dynamic characteristics of non-conventional tmds in multi-degree-of-freedom systems, Iranian Journal of Science and Technology, Transactions of Civil Engineering 44 (1) (2020) 205–215.

[17] M. Zilletti, S. J. Elliott, E. Rustighi, Optimisation of dynamic vibration absorbers to minimise kinetic energy and maximise internal power dissipation, Journal of sound and vibration 331 (18) (2012) 4093–4100.

[18] A. Reggio, M. De Angelis, Optimization of a non-conventional tmd implemented via inter-storey isolation, in: Proc. 9th International Conference on Structural Dynamics-EURODYN, 2014, pp. 1713–1720.

[19] G. Barone, M. Di Paola, F. L. Iacono, G. Navarra, Viscoelastic bearings with fractional constitutive law for fractional tuned mass dampers, Journal of Sound and Vibration 344 (2015) 18–27.

[20] A. Reggio, M. D. Angelis, Optimal energy-based seismic design of non-conventional tuned mass damper (tmd) implemented via inter-story isolation, Earthquake Engineering & Structural Dynamics 44 (10) (2015) 1623–1642.

[21] I. F. Lazar, S. A. Neild, D. J. Wagg, Using an inerter-based device for structural vibration suppression, Earthquake Engineering & Structural Dynamics 43 (8) (2014) 1129–1147.

[22] L. Marian, A. Giaralis, Optimal design of a novel tuned mass-damper–inerter (tmdi) passive vibration control configuration for stochastically support-excited structural systems, Probabilistic Engineering Mechanics 38 (2014) 156–164.

[23] C. Fabrizio, A. M. de Leo, A. Di Egidio, Tuned mass damper and base isolation: a unitary approach for the seismic protection of conventional frame structures, Journal of Engineering Mechanics 145 (4) (2019) 04019011.

[24] S. H. Crandall, W. D. Mark, Random vibration in mechanical systems, Academic Press, 2014.

[25] S. Adhikari, On the quantification of damping model uncertainty, Journal of Sound and Vibration 306 (1-2) (2007) 153–171.

[26] S. Adhikari, M. Friswell, K. Lonkar, A. Sarkar, Experimental case studies for uncertainty quantification in structural dynamics, Probabilistic Engineering Mechanics 24 (4) (2009) 473–492.

[27] S. Chowdhury, S. Adhikari, In-sample versus ensemble optimisation of tuned mass dampers for structures with uncertainties, Probabilistic Engineering Mechanics (2026) 103982.

[28] S. Adhikari, Equivalent damping and closed-form response statistics of stochastic oscillators, Probabilistic Engineering Mechanics (2026) 104015.

[29] H. Yu, F. Gillot, M. Ichchou, Reliability based robust design optimization for tuned mass damper in passive vibration control of deterministic/uncertain structures, Journal of Sound and Vibration 332 (9) (2013) 2222–2238.

[30] I. Venanzi, Robust optimal design of tuned mass dampers for tall buildings with uncertain parameters, Structural and Multidisciplinary Optimization 51 (1) (2015) 239–250.

[31] D. Li, H. Tang, S. Xue, Robust design of tuned mass damper with hybrid uncertainty, Structural Control and Health Monitoring 28 (10) (2021) e2803.

[32] L. Meirovitch, Fundamentals of vibrations, Waveland Press, 2010.

[33] Y. Ikeda, Fundamental equation based on pole allocation for interstory seismic isolation of buildings, Structural Control and Health Monitoring 28 (3) (2021) e2687.

[34] Y. Ikeda, Y. Matsumoto, Unified description of passive vibration control for buildings based on pole allocation applied to three-degree-of-freedom model, Structural Control and Health Monitoring 29 (9) (2022) e2995.

[35] Y. Ikeda, N. Uhara, Application of pole allocation to optimize passive viscous dampers represented by the maxwell model, Soil Dynamics and Earthquake Engineering 188 (2025) 109037.

[36] G. Casella, R. Berger, Statistical inference, Chapman and Hall/CRC, 2024.

[37] P. Billingsley, Probability and Measure, anniversary edition Edition, Wiley, 2012.